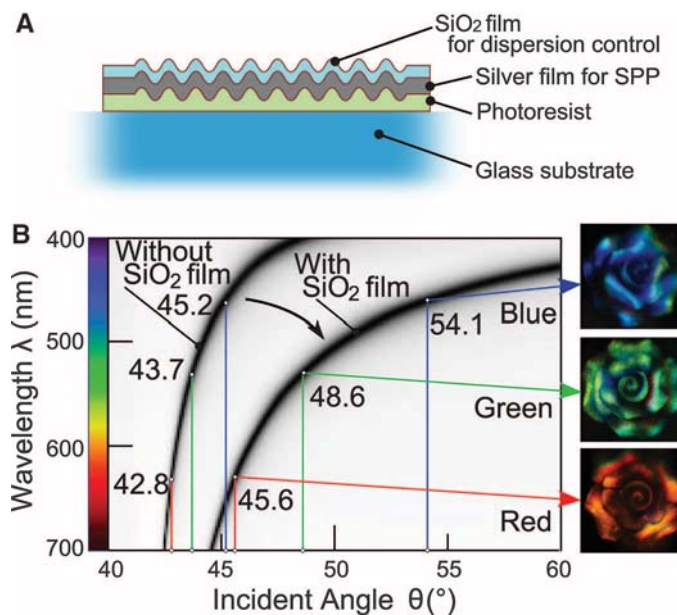**Fig. 3.** Multilayer system and the color dispersion of an SPP hologram. (**A**) Hologram configuration. From the top, dielectric layer (25-nm-thick SiO₂), metal layer (55-nm-thick silver), and dielectric substrate with 25-nm depth modulation (150-nm-thick photoresist on the glass). (**B**) The top SiO₂ layer works for expanding the color dispersion to incident angle. Without the SiO₂ layer on the hologram, the angular separation for color reconstruction is small. Rose pendants of red, green, and blue are separated in the reconstruction, as shown in the insets.

References and Notes

1. J. Heber, *Nature* **461**, 720 (2009).
2. H. Raether, *Surface Plasmons on Smooth and Rough surfaces and on Gratings* (Springer, Berlin, 1988).
3. S. Kawata, *Near Field Optics and Surface Plasmon Polaritons* (Springer, Berlin, 2001).
4. B. Liedberg, C. Nylander, I. Lunström, *Sens. Actuators* **4**, 299 (1983).
5. H. Kano, S. Kawata, *Opt. Lett.* **21**, 1848 (1996).
6. V. E. Ferry, L. A. Sweatlock, D. Pacifici, H. A. Atwater, *Nano Lett.* **8**, 4391 (2008).
7. T. Okamoto, F. H'Dhili, S. Kawata, *Appl. Phys. Lett.* **85**, 3968 (2004).
8. N. I. Zheludev, S. L. Prosvirnin, N. Papasimakis, V. A. Fedotov, *Nat. Photonics* **2**, 351 (2008).
9. S. Kawata, Y. Inouye, P. Verma, *Nat. Photonics* **3**, 388 (2009).
10. N. Hayazawa, Y. Inouye, Z. Sekkat, S. Kawata, *Opt. Commun.* **183**, 333 (2000).
11. J. B. Pendry, *Phys. Rev. Lett.* **85**, 3966 (2000).
12. N. Fang, H. Lee, C. Sun, X. Zhang, *Science* **308**, 534 (2005).
13. C. Loo, A. Lowery, N. Halas, J. West, R. Drezek, *Nano Lett.* **5**, 709 (2005).
14. J. J. Cowan, *Opt. Commun.* **5**, 69 (1972).
15. S. Maruo, O. Nakamura, S. Kawata, *Appl. Opt.* **36**, 2343 (1997).
16. G. P. Wang, T. Sugiura, S. Kawata, *Appl. Opt.* **40**, 3649 (2001).
17. M. Ozaki, J. Kato, R. Furutani, S. Kawata, *J. Jpn. Soc. Precision Eng.* **74**, 1113 (2008).
18. Materials and methods are available as supporting materials on *Science* Online.
19. Yu. N. Denisyuk, *Sov. Phys. Dokl.* **7**, 543 (1962).
20. S. A. Benton, *J. Opt. Soc. Am.* **59**, 1545 (1969).
21. O. Bryngdahl, *J. Opt. Soc. Am.* **59**, 1645 (1969).
22. S. Kawata conceived the research and planned the experiments. M. Ozaki conducted the experiment and calculations. All authors discussed the results and contributed in preparing the manuscript. The authors thank R. Furutani for discussion and P. Verma for his review.

comes as large as 10° due to the higher index n_m of film; more precisely, the angles for the three colors are at 45.6°, 48.6°, and 54.1°, respectively. In Fig. 3B, theoretical curves are plotted from the calculation of a multilayer system based on Fresnel's equations for noncoated and coated SPP holograms. A rose pendant in the figure is decomposed into three colors in reconstruction by choosing the angle for white-light illumination (Fig. 3B).

Our results show that plasmon color holography provides a view of an object or a scene seen naturally and vitally with white-light illumination. A typical amplitude modulation in plasmon hologram is ~25 nm (fig. S2), which is much

thinner compared with Lippmann-Denisyuk's color hologram (*19*) based on Bragg diffraction in volume. The rainbow holograms mounted, for example, on credit cards (*20*) also reconstruct with white light, where color varies with viewing angle but not with the color distribution in the object. Plasmon holography is advantageous in terms of background-beam–free reconstruction because the illumination light is totally reflected back at the hologram (*21*). Plasmon holography does not suffer from the ghost produced by the diffraction of ambient light or higher orders of diffraction, because those components are not coupled with SPPs.

The Hot Summer of 2010: Redrawing the Temperature Record Map of Europe

David Barriopedro,[1]* Erich M. Fischer,[2] Jürg Luterbacher,[3] Ricardo M. Trigo,[1] Ricardo García-Herrera[4]

The summer of 2010 was exceptionally warm in eastern Europe and large parts of Russia. We provide evidence that the anomalous 2010 warmth that caused adverse impacts exceeded the amplitude and spatial extent of the previous hottest summer of 2003. "Mega-heatwaves" such as the 2003 and 2010 events likely broke the 500-year-long seasonal temperature records over approximately 50% of Europe. According to regional multi-model experiments, the probability of a summer experiencing mega-heatwaves will increase by a factor of 5 to 10 within the next 40 years. However, the magnitude of the 2010 event was so extreme that despite this increase, the likelihood of an analog over the same region remains fairly low until the second half of the 21st century.

Increasing greenhouse gas concentrations are expected to amplify the variability of summer temperatures in Europe (*1–5*). Along with mean warming, enhanced variability results in more frequent, persistent, and intense heatwaves

(*6–10*). Consistent with these expectations, Europe has experienced devastating heatwaves in recent years. The exceptional summer of 2003 (*1, 11–13*) caused around 70,000 heat-related deaths, mainly in western and central Europe

(*14*). In summer 2010, many cities in eastern Europe recorded extremely high values of daytime (for example, Moscow reached 38.2°C), nighttime (Kiev reached 25°C), and daily mean (Helsinki reached 26.1°C) temperatures (fig. S1). Preliminary estimates for Russia referred a death toll of 55,000, an annual crop failure of ~25%, more than 1 million ha of burned areas, and ~US$15 billion (~1% gross domestic product) of total economic loss (*15*). During the same period, parts of eastern Asia also experienced extremely warm temperatures, and Pakistan was hit by devastating monsoon floods.

In order to characterize the magnitude and spatio-temporal evolution of the 2010 event in a historical context, we used daily mean data sets

[1]Instituto Dom Luiz, University of Lisbon, 1749-016 Lisbon, Portugal. [2]Institute for Atmospheric and Climate Science, Eidgenössische Technische Hochschule (ETH) Zurich, 8092 Zurich, Switzerland. [3]Department of Geography, Justus-Liebig-University of Giessen, D-35390 Giessen, Germany. [4]Agencia Estatal de Meteorología (AEMET), 28071 Madrid, Spain.

*To whom correspondence should be addressed. E-mail: dbarriopedro@fc.ul.pt

from the two longest reanalyses, which together extend back to 1871 (*15–17*). The spatial pattern of the maximum summer temperature anomalies (Fig. 1, A to D) reveals that western Russia was in the center of the exceptional warmth at all temporal scales. Weekly to monthly anomalies were particularly pronounced, exceeding the 1970–1999 mean (*18*) by 10°C—more than 4 standard deviations (SDs). According to reanalyses, other countries (Baltic countries, Belarus, Ukraine, and Kazakhstan) also experienced extreme temperatures that broke the summer records of the last 140 years at many temporal scales [supporting online material (SOM) text].

Figure 1E displays the temporal evolution of areas that were simultaneously affected by record-breaking anomalies for any summer period of 1- to 91-day length. At short time scales (daily to fortnightly), new historical maxima were first observed in late July 2010 and persisted until the second week of August. During that time, extensive fires across western Russia killed 53 people and made 3500 people homeless, and Moscow suffered a devastating rise in mortality, smoke fire, and air pollution (*15*). The record-breaking pattern is not symmetric in time, indicating that warm conditions had started already in July and ended abruptly by mid-August. Be-

tween mid-July and early August, a record-scale area of more than 2 million km^2 registered unprecedented anomalies at the 15- to 61-day time scales. These results reflect the extraordinary nature of the 2010 event and confirm that most of the record-breaking values highlighted in Fig. 1, A to D, occurred simultaneously.

The most evident features associated with the 2010 event were (i) quasi-stationary anticyclonic circulation anomalies over western Russia (fig. S5) and (ii) deficit of January-to-July 2010 accumulated precipitation and early spring snow cover disappearance in western-central Russia (fig. S6). High-pressure systems are well-known to produce warm conditions at surface by enhancing subsidence, solar heating, and warm-air advection (*19–21*). The lack of water availability results in a continuous reduction of soil moisture and enhanced sensible heat fluxes that exacerbate the strength of summer heatwaves (*20–22*).

Unlike 2010, the summer of 2003 was characterized by two extreme periods (centered on 15 June and the first fortnight of August) (*12*) that contributed to the rise of the number of locations with temperatures beyond their historical maxima at seasonal time scales. However, the 2010 event exceeded the 2003 episode in terms of amplitude and spatial extent. Thus, the maximum extension of areas experiencing record-breaking temperatures in 2003 was ~1 million km^2, which is considerably lower than that of 2010. The intensity of the 2003 event was also ~1 to 2 SDs weaker for most of the subseasonal time scales (fig. S7).

Despite the distinctive spatio-temporal evolution of the 2003 and 2010 events, their record-breaking anomalies reached comparable amplitude and extension at seasonal scales. Therefore, from a seasonal perspective it is interesting to compare these events at continental scales. Herein, surface temperature analysis data (*23*) and multiproxy surface air temperature reconstructions since 1500 (*11*) are used to place these recent extreme European summers in a palaeoclimatic context (*15*). Figure 2 displays the European mean summer land surface air temperature distribution for the 1500–2010 period. The European mean 2010 summer [temperature anomaly (ΔT) = +1.8°C, 3.5 SDs relative to 1970–1999] was ~0.2°C warmer than the previous warmest summer of 2003 (*11*). This number is even more noticeable if we consider that the European average temperature is defined for the land area [35°N, 70°N] and [25°W, 40°E], thus excluding many regions affected by outstanding temperatures in 2010. Further, the historical evolution of the hottest summers in Europe (Fig. 2, bottom) suggests that the last decade stands substantially above any other 10-year period since 1500. Taking into account the uncertainties in the reconstruction (*11*, *15*), we found that at least two summers in this decade have most likely been the warmest of the last 510 years in Europe.

Figure 3 further stresses the exceptional magnitude of the 2010 summer, displaying the amplitude
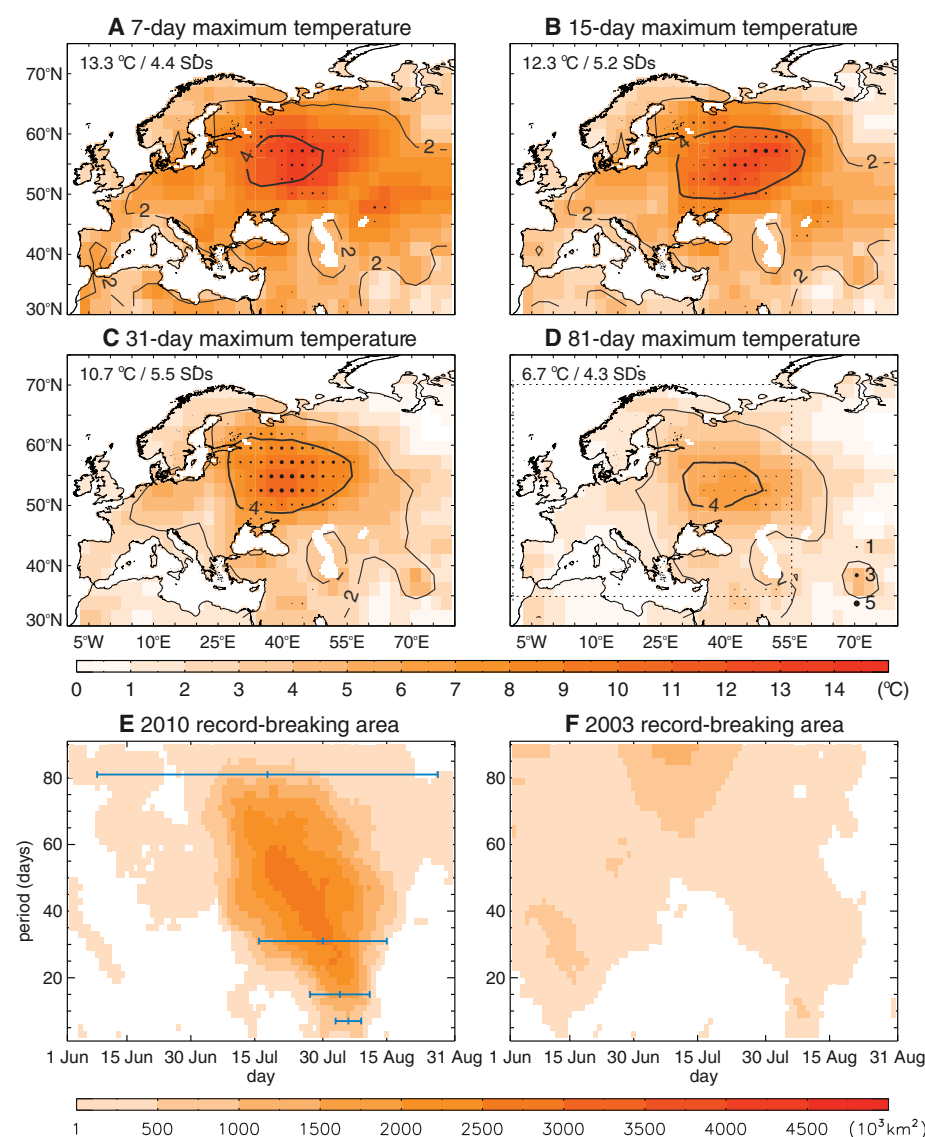

Fig. 1. Spatio-temporal evolution of the 2010 summer. Shown are maximum temperature anomalies (degrees Celsius, relative to 1970–1999) in summer 2010 for (**A**) 7-day, (**B**) 15-day, (**C**) 31-day, and (**D**) 81-day average periods. Contour lines indicate the anomaly divided by the corresponding SD of all summer days of the reference period. Black points highlight record-breaking values, the size being proportional to exceedance over the previous maximum. The maximum record-breaking temperature anomaly is shown in the top left corner. (**E** and **F**) Temporal evolution of the spatial extent (in 10^3 km^2) of areas experiencing record-breaking temperatures at different time scales during summer 2010. Only those land regions within the box of (D) are considered. Blue bars indicate the period of maximum extension for the time scales represented in (A) to (D). Data are from (*17*) (1871–1947) and (*16*) (1948–2010).

Fig. 2. European summer temperatures for 1500–2010. Statistical frequency distribution of best-guess reconstructed and instrument-based European ([35°N, 70°N], [25°W, 40°E]) summer land temperature anomalies (degrees Celsius, relative to the 1970–1999 period) for the 1500–2010 period (vertical lines). The five warmest and coldest summers are highlighted. Gray bars represent the distribution for the 1500–2002 period (*11*), with a Gaussian fit in black. Data for the 2003–2010 period are from (*23*). (Bottom) The running decadal frequency of extreme summers, defined as those with temperature above the 95th percentile of the 1500–2002 distribution. A 10-year smoothing is applied. Dotted line shows the 95th percentile of the distribution of maximum decadal values that would be expected by random chance (*15*).
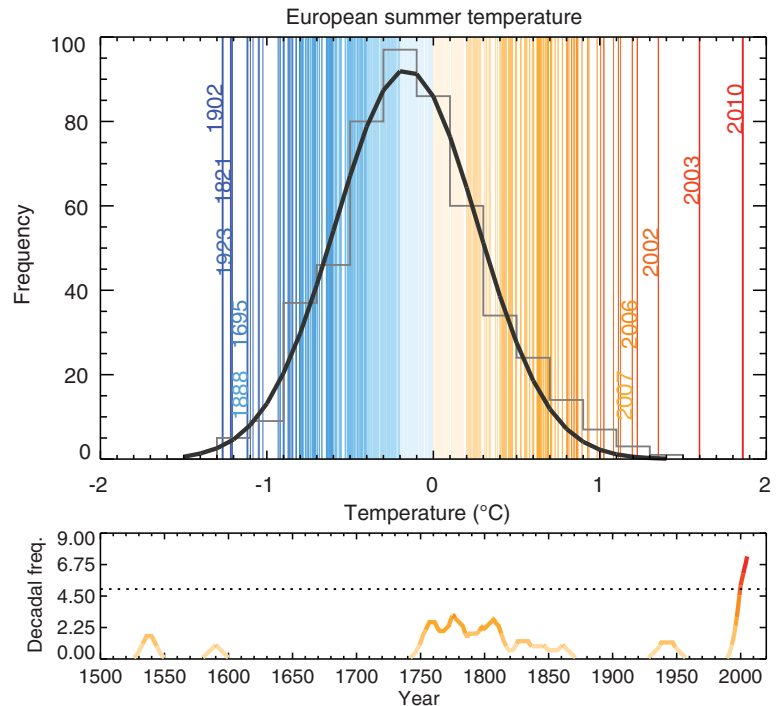

European summer temperature

Fig. 3. Spatial distribution of the hottest European summers (*24*). The height and the color of the bars indicate the best-guess maximum anomaly (degrees Celsius, relative to the 1970–1999 period) and the decade of the corresponding summer, respectively, for the periods (**A**) 1500–2000 and (**B**) 1500–2010. For better readability, each bar is subdivided with 1°C intervals. The embedded plot shows the corresponding percentage of European areas with summer maxima above the given temperature (in SDs) for the 1500–2000 (dashed line) and 1500–2010 (dotted line) periods. Data sources are (*11*) (1500–2002) and (*23*) (2003–2010).


Record-breaking summers
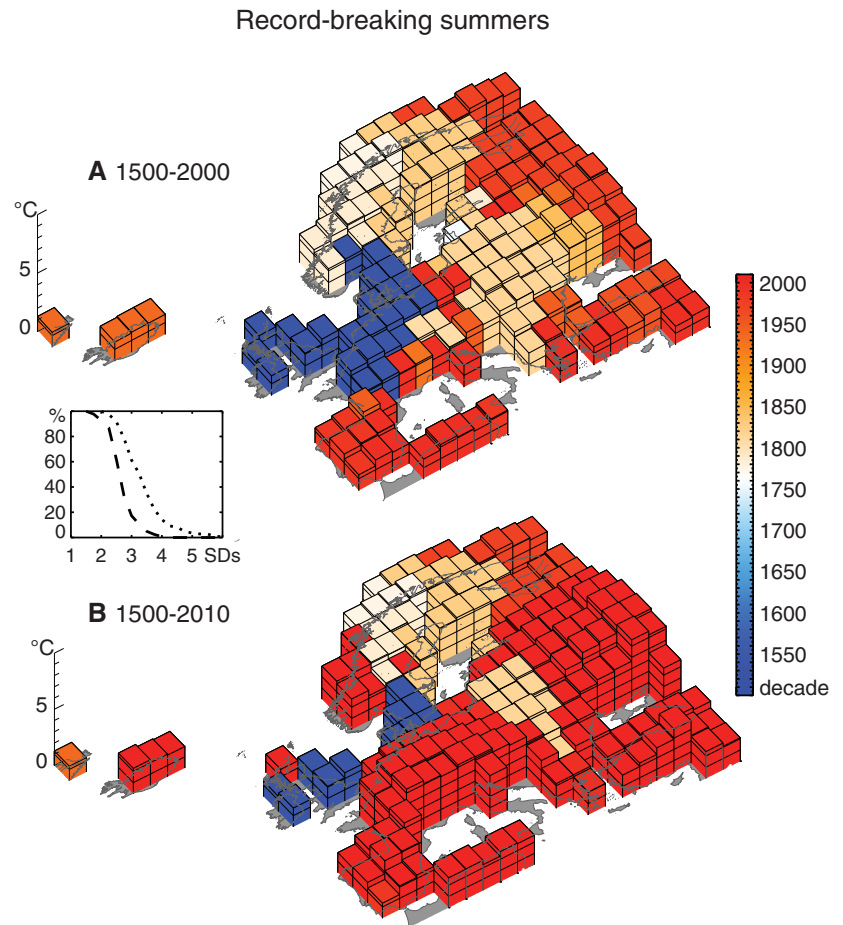
of the hottest summers across Europe and the decade when they occurred (*24*). To highlight the contribution of summers in the 2001–2010 dec-ade, the analysis was initially restricted to the 1500–2000 period (Fig. 3A) and then updated to 2010 (Fig. 3B). Until the end of the 20th century (20C), maximum seasonal temperatures across Europe mostly ranged 2 to 3 SDs of their 1970–1999 climatology, with regional extreme summers

Fig. 4. Multi-model projections of mega-heatwaves. Return periods (years) of 7-day summer maximum regional temperature for three 30-year periods and 11 RCMs forced with A1B emission scenario (26) over (**A** to **C**) EE ([52.5°N, 60°N]; [27.5°E, 40°E]) and (**D** to **F**) WE ([42.5°N, 50°N]; [0°E, 15°E]). Anomalies are depicted as SDs of the control period 1970–1999. Shading indicates the degree of agreement between models as measured by the overlapping of their 95% confidence interval limits. Dotted lines comprise the 75% density distribution, with the median in between. Black lines represent the corresponding fit from reanalysis (16). Blue and green dots represent the RCM-projected distribution of RPs for a 2010- and a 2003-like event, respectively, with the size proportional to the level of model agreement. The vertical mark indicates the best guess, as obtained from the median of the RCM distribution.
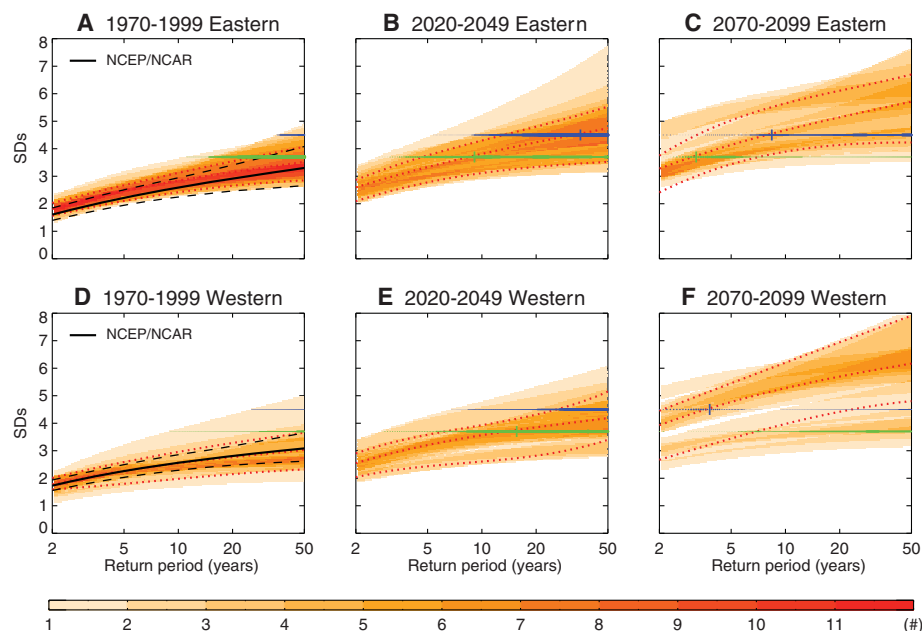
clustering in a few decades of the last five centuries. During the 2001–2010 decade, 500-year-long records were likely broken over ~65% of Europe, including eastern Europe (2010), southwestern-central Europe (2003), the Balkans (2007), and Turkey (2001). These summers have considerably contributed to the upper tail of the European distribution of summer maxima (Fig. 3, inset). Thus, the percentage of European regions with seasonal maxima above 3 SDs (>99th percentile of the 1970–1999 distribution) has doubled within one decade. The 2003 and 2010 summers were likely the warmest on record over ~25% of Europe, standing as major contributors to the current European map of the hottest summers.

It is noticeable that the two hottest summers in Europe resulted from subseasonal heatwaves of outstanding magnitude and large spatial extent. This raises the question of whether these "mega-heatwaves" (25) (and regional extreme events at other time scales) will become more frequent in the future. To address this question, we evaluated transient experiments from 11 high-resolution regional climate models (RCMs) driven with different general circulation models (GCMs), which are forced with the A1B emission scenario (15, 26). The analysis emphasizes analogs of the 2010 and 2003 events over the eastern (EE) and western (WE) European regions that were strongly affected by these mega-heatwaves (fig. S11).

Anthropogenic changes are assessed in terms of return periods (RPs) of maximum 7-day summer regional temperature for three time slices (1970–1999, 2020–2049, and 2070–2099) (Fig. 4). Regional mean temperatures were normalized with reference to the 1970–1999 climatology and hereafter expressed as SDs (27). Simulations for the 1970–1999 period indicate a reasonable model skill, although there is a considerable spread of model results, particularly for long RPs (figs. S12 and S13). The ensemble of RCMs projects that

weekly heat spells of the magnitude of the second week of August 2003 (7-day anomaly of 3.7 SDs), which are extremely rare in the 20C simulations, will probably occur in 2020–2049, with a best-guess RP of ~10 years in EE and ~15 years in WE. However, a weekly 2010-like event (~4.5 SDs) remains very rare in the same period (best-guess RPs of >30-year over both regions). By the end of the 21st century (21C), such extreme weekly heat spells are expected every ~8 years in EE and ~4 years in WE, whereas some models show regular 2003-like anomalies (about every second summer). The estimated RPs involve major model uncertainties and should be carefully interpreted, given the high natural variability of such extreme events. Thus, some RCMs show several events similar to 2010 in the period 2020–2049 (fig. S14, left), whereas others show just one event similar to 2003 within the last 30 years of the 21C (fig. S14, right).

The increase in probability of 2003- and 2010-type events depends on the time scale addressed and differs if the seasonal anomaly is emphasized instead of the weekly time scale above (SOM text). The analysis of RCM time series for the 2011–2100 period reveals 2003 analogs (at all 7- to- 91-day temporal scales) before 2050 in more than half of the models (figs. S14 and S15). However, the same cannot be stated for a 2010 analog until the second half of the 21C, particularly at monthly and seasonal scales. For the last 30 years of the 21C, the occurrence of 2010-like monthly anomalies (~5 SDs) increases rapidly to one event per decade in most models, and by 2100 all models present at least one summer like 2010.

The enhanced frequency for small to moderate anomalies of 2 to 3 SDs is mostly accounted for by a shift in mean summer temperatures (compare Fig. 4 with fig. S18). However, the future probabilities of mega-heatwaves with SDs sim-

ilar to 2003 and 2010 are substantially amplified by enhanced variability. Particularly in WE, variability has been suggested to increase at interannual and intraseasonal time scales (1, 2) as a result of increased land-atmosphere coupling (28) and changes in the surface energy and water budget (2, 29). Models indicate that the structure of circulation anomalies associated with mega-heatwaves remains essentially unchanged in the future (SOM text).

Our results reveal that along with the reported changes in local heatwaves (8), there is an increasing likelihood of mega-heatwaves over highly populated areas of Europe with magnitudes such that they would exceed the exceptional current weekly-to-seasonal temperature maxima of WE within the next four decades and of EE afterwards. Given the disastrous effects of the 2003 and 2010 events, these results venture serious risks of simultaneous adverse impacts over large areas if no adaptive strategies are adopted.

References and Notes
1. C. Schär et al., Nature **427**, 332 (2004).
2. E. M. Fischer, C. Schär, Clim. Dyn. **33**, 917 (2009).
3. J. H. Christensen et al., in Climate Change 2007: The Physical Science Basis. Contribution of Working Group I to the Fourth Assessment Report of the Intergovernmental Panel on Climate Change, S. Solomon et al., Eds. (Cambridge Univ. Press, New York, 2007).
4. F. Giorgi, X. Q. Bi, J. Pal, Clim. Dyn. **23**, 839 (2004).
5. A. Klein-Tank, G. Können, F. Selten, Int. J. Climatol. **25**, 1 (2005).
6. P. M. Della-Marta, M. R. Haylock, J. Luterbacher, H. Wanner, J. Geophys. Res. **112**, (D15), D15103 (2007).
7. G. A. Meehl, C. Tebaldi, Science **305**, 994 (2004).
8. E. M. Fischer, C. Schär, Nat. Geosci. **3**, 398 (2010).
9. M. Beniston et al., Clim. Change **81**, (S1), 71 (2007).
10. F. G. Kuglitsch et al., Geophys. Res. Lett. **37**, L04802 (2010).
11. J. Luterbacher, D. Dietrich, E. Xoplaki, M. Grosjean, H. Wanner, Science **303**, 1499 (2004).
12. R. García-Herrera, J. Díaz, R. M. Trigo, J. Luterbacher, E. M. Fischer, Crit. Rev. Environ. Sci. Technol. **40**, 267 (2010).

13. E. Black, M. Blackburn, G. Harrison, B. Hoskins, J. Methven, *Weather* **59**, 217 (2004).
14. J. M. Robine *et al.*, *C. R. Biol.* **331**, 171 (2008).
15. Materials and methods are available as supporting material on *Science* Online.
16. R. Kistler *et al.*, *Bull. Am. Meteorol. Soc.* **82**, 247 (2001).
17. G. P. Compo *et al.*, *Q. J. R. Meteorol. Soc.* **137**, 1 (2011).
18. For coherence with model results, and because of the limited availability of data in some models, 1970–1999 is used as the reference period throughout this manuscript. Summer includes all days from 1 June to 31 August.
19. R. M. Trigo, R. García-Herrera, J. Díaz, I. F. Trigo, M. A. Valente, *Geophys. Res. Lett.* **32**, L10701 (2005).
20. E. Xoplaki, J. F. González-Rouco, J. Luterbacher, H. Wanner, *Clim. Dyn.* **20**, 723 (2003).
21. E. M. Fischer, S. I. Seneviratne, D. Lüthi, C. Schär, *Geophys. Res. Lett.* **34**, L06707 (2007).
22. R. Vautard *et al.*, *Geophys. Res. Lett.* **34**, L07711 (2007).
23. J. Hansen, R. Ruedy, J. Glascoe, M. Sato, *J. Geophys. Res.* **104**, (D24), 30997 (1999).
24. Figure 3 and the accompanying text are based on best-guess temperature reconstructions with relatively large uncertainties at regional and gridpoint scales and should therefore be interpreted with caution and not be overemphasized.
25. The concept of mega-heatwave is herein used to refer to regional mean temperature anomalies (over ~1 million km²) of extraordinary amplitude (approximately ≥3 SDs relative to the 1970–1999 period) at subseasonal scales (of at least 7 days), thus differing from the classic local heatwave definition.
26. P. van der Linden, J. F. B. Mitchell, "ENSEMBLES: Climate Change and its Impacts: Summary of research and results from the ENSEMBLES project" (Met Office Hadley Centre, Fitzroy Road, Exeter EX1 3PB, UK, 2009).
27. Summer temperature variability is higher in EE, and hence, a given value in SDs actually implies larger anomalies in EE than in WE.
28. S. I. Seneviratne, D. Lüthi, M. Litschi, C. Schär, *Nature* **443**, 205 (2006).
29. G. Lenderink, A. van Ulden, B. van den Hurk, E. van Meijgaard, *Clim. Change* **81**, (S1), 233 (2007).
30. Acknowledgements. This study was supported by the EU/FP6 project CIRCE (#036961) (D.B., J.L., R.T., and R.G.), the Instituto Dom Luiz–Faculdade de Ciências da Universidade de Lisboa project ENAC (PTDC/AAC-CLI/103567/2008) (D.B., R.T.), the Swiss National Science Foundation (Swiss National Center of Competence in Research–Climate) (E.F.), the EU/FP7 project ACQWA (#212250) (J.L.), the Deutsche Forschungsgemeinschaft project PRIME (LU1608/1-1, AOBJ: 568460) within the Priority Program 'INTERDYNAMIK' (J.L.), the project "Historical climatology of the Middle East based on Arabic sources back to ad 800" (LU 1608/2-1 AOBJ 575150) (J.L.) and the project "Climate Change and Extreme Weather in Hesse–Analysis of observation data and ensemble projections for the 21st century" funded by the Hessian Centre on Climate Change and Geology (J.L.). The ENSEMBLES data used in this work was funded by the European Union/FP6 project ENSEMBLES (#505539), whose support is gratefully acknowledged. 20th Century and National Centers for Environmental Prediction (NCEP)/National Center for Atmospheric Research (NCAR) reanalyses data were provided by the National Oceanic and Atmospheric Administration (NOAA)/Office of Oceanic and Atmospheric Research (OAR)/Earth System Research Laboratory (ESRL) Physical Sciences Division, Boulder, Colorado, USA, from their Web site at www.esrl.noaa.gov/psd/.

13C NMR Guides Rational Design of Nanocatalysts via Chemisorption Evaluation in Liquid Phase

Karaked Tedsree,[1] Chun Wong Aaron Chan,[1] Simon Jones,[1] Qian Cuan,[2] Wei-Kun Li,[2] Xue-Qing Gong,[2] Shik Chi Edman Tsang[1]*

The search for more efficient heterogeneous catalysts remains critical to the chemical industry. The Sabatier principle of maximizing catalytic activity by optimizing the adsorption energy of the substrate molecule could offer pivotal guidance to otherwise random screenings. Here we show that the chemical shift value of an adsorbate (formic acid) on metal colloid catalysts measured by ^{13}C nuclear magnetic resonance (NMR) spectroscopy in aqueous suspension constitutes a simple experimental descriptor for adsorption strength. Avoiding direct contact between the ^{13}C atom and the metal surface eliminates peak broadening that has confounded prior efforts to establish such correlations. The data can guide rational design of improved catalysts, as demonstrated here for the cases of formic acid decomposition and formic acid electro-oxidation reactions.

I n 1913, the French chemist Paul Sabatier introduced a qualitative concept in chemical catalysis that described the appropriate interaction between catalyst and substrate as a balance between extremes. If the interaction is too weak, the substrate will fail to bind to the catalyst and no reaction will take place; if it is too strong, the catalyst will be blocked by the substrate, intermediate, or product, hindering turnover of the catalytic cycle (*1*). The Sabatier principle is best illustrated by Balandin's volcano relations between reaction rates and adsorption energies, which was employed from the study of catalytic decomposition of formic acid over transition metals by Sachtler and Fahrenfort in 1961 (*2*). However, various thermodynamic data, such as the heat of formate or oxide formation, were actually used to estimate the adsorption energies in these early studies. These bulk thermodynamic properties established under different reaction conditions were not the best descriptors for surface adsorption structures and energies (*3*). Over the past decade, theoretical calculation of adsorption energies on solid surfaces using density functional theory (DFT) has become practical on account of enhanced computing power, although data to validate this complex modeling under realistic reaction conditions [in liquid phase or under pressure, rather than in ultrahigh vacuum (UHV)] have been scarce (*4*). In addition, Somorjai earlier demonstrated that face specific-

ity is a characteristic property of adsorption (*5*), which implies that the modeling of working catalysts that comprise different surfaces while taking complexities such as solvent effects, surface specificity, and adsorbate-adsorbate interactions into account may not be a simple task.

Traditional resonance methods such as electron spin resonance (ESR) and nuclear magnetic resonance (NMR) can yield a wealth of information about the electronic interactions between atoms under non-UHV conditions in the liquid or solid phase (*6, 7*). Studies of chemisorption of small probing molecules such as CO and ethylene on metal surfaces by both solution and solid-phase NMR have been reported (*8–13*). A broad NMR peak was observed because of particle anisotropy and magnetic field inhomogeneity. Newmark (*12*) and Bradley (*13*) used solution-phase ^{13}C NMR to probe adsorption of ^{13}CO onto different metal colloids in solution. They showed that the tumbling motion of nanosized metal particles in solution is sufficiently fast to reduce the particle anisotropy in a magnetic field over the liquid suspension of particles. However, all of the above works encountered significant Knight-shift effects in their NMR peaks due to the coupling of conduction electrons from the Fermi levels of the metal particles with the probe ^{13}C atom in direct contact, which severely perturbed and broadened the ^{13}C chemical shift values [peak position and peak width are affected, ranging from a few to hundreds of parts per million (ppm)]. This problem precluded the potential use of chemical shift values for assessing adsorption strength until our initial work on the adsorption of formic acid on Ru nanoparticles. We showed that the presence of the O spacer atoms in the adsorbed formate substantially reduces the Knight-shift effect on the ^{13}C nucleus, because it is not directly coupled to the

[1]Wolfson Catalysis Centre, Department of Chemistry, University of Oxford, Oxford OX1 3QR, UK. [2]Labs for Advanced Materials, Research Institute of Industrial Catalysis, East China University of Science & Technology, Shanghai 200237, P. R. China.

*To whom correspondence should be addressed. E mail: edman.tsang@chem.ox.ac.uk